PERGAMON

Available online at www.sciencedirect.com

SCIENCE DIRECT®

Electrochimica Acta 48 (2003) 791–797

ELECTROCHIMICA Acta

www.elsevier.com/locate/electacta

# Naphthalene sulfonate formaldehyde (NSF)-resin derived carbon beads as an anode material for Li-ion batteries

Masaki Yoshio [a,*], Hongyu Wang [a,1], Yun Sung Lee [a], Kenji Fukuda [b]

[a] *Department of Applied Chemistry, Saga University, 1 Honjo, Saga 840-8502, Japan*
[b] *Research Center, Mitsui Mining Co. Ltd., Wakamatsu-ku, Kitakyushu 808-0021, Japan*

Received 23 August 2002; received in revised form 12 November 2002

**Abstract**

Carbon beads have been prepared by the carbonization of naphthalene sulfonate formaldehyde (NSF) resin. The procedures for the preparation have been described in detail. The electrochemical performance of NSF carbon beads as an anode material for lithium batteries has been correlated with some carbonization factors such as the molecular weight of the precursor, the ramp rate, and final temperature, etc.


*Keywords:* Lithium-ion battery; Hard carbon, anode material; Carbon beads; Carbonization

## 1. Introduction

In recent years, carbonaceous materials have drawn significant attentions as anode materials in lithium-ion batteries. Among so many kinds of carbonaceous materials, graphite has been extensively used in lithium-ion batteries on the market nowadays mainly because of its flat and low voltage range, and its good cycle performance in compatible electrolytes [1,2]. However, its reversible capacity is limited to the theoretical value of 372 mA h $g^{-1}$ ($LiC_6$), which may frustrates its further use. From the viewpoint of reversible capacity, the most promising successor to graphite in the big family of carbonaceous materials may be disordered carbon, which has a much higher capacity [3–5].

Many disordered carbons have been prepared by the carbonization of some polymer precursors such as phenol and furan resins at low temperatures. naphthalene sulfonate formaldehyde (NSF) condesate ammonium salt is a suitable carbon precursor by virtue of the high carbon content, the absence of metallic impurities, and feasibility to make NSF into different forms like fiber, beads, etc. In fact, the morphology of carbon is a key factor in practical lithium-ion batteries. Carbon particles in sphere shape draw considerable attention because of the following merits: (1) they possess the smallest surface area given certain density, which can reduce the irreversible capacity comes from decomposition of the electrolytes on their surface; (2) they can be easily spread with binder on the copper substrate thinly and evenly; (3) their isotropic physical properties allow for higher rate capacity; etc. Therefore, NSF resin was processed into carbon beads as an anode material for lithium-ion batteries in this study.

In this paper, we will describe the procedures for preparation of NSF carbon beads. The electrochemical performance of NSF carbon beads is also investigated.

## 2. Experimental

### 2.1. Synthesis of NSF

The whole process of the synthesis is shown in Fig. 1. At first, 95% naphthalene was melted in a glass flask equipped with reflux condenser, and then 98% $H_2SO_4$ was dipped into the flask in the mole ratio of 1–1.05

* Corresponding author. Fax: +81-952-28-591
*E-mail address:* yoshio@ccs.ce.saga-u.ac.jp (M. Yoshio).
[1] Present address: Department of Energy and Hydrocarbon Chemistry, Graduate School of Engineering, Kyoto University, Kyoto 606-8501, Japan.

0013-4686/02/$ - see front matter © 2002 Elsevier Science Ltd. All rights reserved.
PII: S0013-4686(02)00748-X

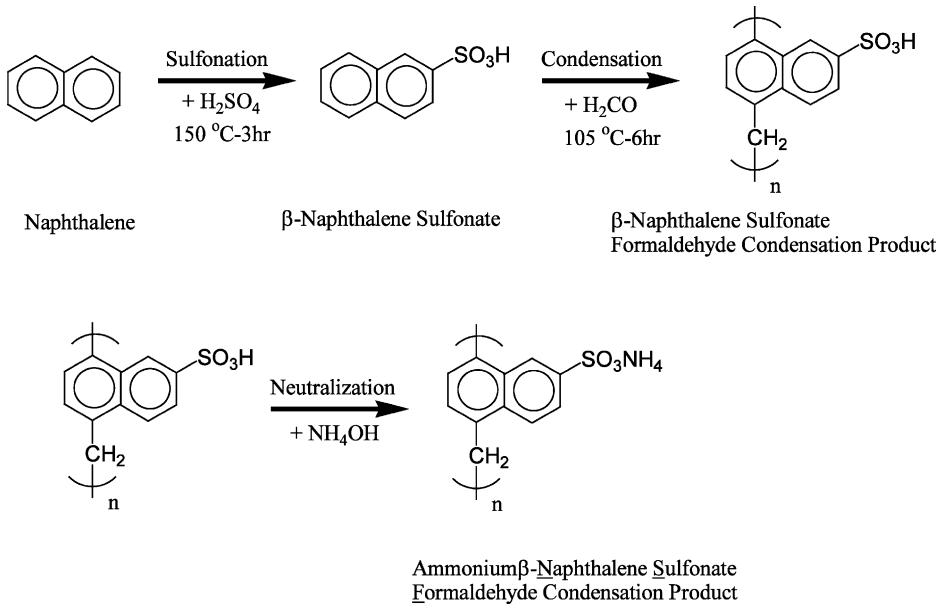


Fig. 1. Process of the synthesis for NSF.

(naphthalene to $H_2SO_4$). The temperature of the flask was kept under 115 °C during the course of $H_2SO_4$ addition. After the addition of $H_2SO_4$, the flask was heated at 150 °C for 3 h and the sulfonation of naphthalene took place. After the sulfonation, the unreacted naphthalene and the resultant water were get rid of by reduced pressure distillation. Then formaldehyde was dipped into the flask in the mole ratio of 1–1.05 (naphthalene to formaldehyde) and the temperature was kept under 105 °C. After that, the flask was held at this temperature for over 6 h and the condensation reaction proceeded. With the progress of condensation, the viscosity of the product in the flask increased and the stirring became difficult. For homogeneous condensation in the product, hot water was added into the flask to make the stirring easy. After the condensation, the product was neutralized by ammonia water. The neutralization product was passed through the filter paper and the over-condensed gel was separated, NSF aqueous solution thus obtained was employed as the precursor for hard carbon.

### 2.2. Sphere and carbonization of NSF

NSF spheres was made from NSF aqueous solution by sprayed-layer drying. In this process, NSF aqueous solution was sprayed into the drying cylinder by an atomizer, hot air flowed through the cylinder, dried spheric NSF solid particles could be obtained. The NSF spheres were then carbonized in $N_2$ atmosphere at different temperatures higher than 550 °C. The obtained carbon spheres were called as 'carbon beads'.

### 2.3. Evaluation of NSF

Elemental analysis of NSF for C, H, N and S was carried out using a Heraus Analyser. Molecular weight of NSF was estimated by gel permeation chromatography (Shimazu, LC-6), which contained the column G300SWXL from Tohso. The mixed solvents of $H_2O$–acetonitrile were used. The thermal gravimetric and mass analysis of NSF was performed by TG50-GCMS-QP1000, while TAS300TG/DSC (Rigaku) was applied in the Differential Scanning Calorimetry (DSC) studies. In both the cases above, the ramp rate was 10 °C $min^{-1}$ and the flow rate of $N_2$ was 100 ml $min^{-1}$.

### 2.4. Electrochemical characterization of NSF carbon beads

The carbon electrodes were prepared by evenly and thinly spreading a slurry mixture of carbon beads (91 wt.%) and PVDF (9 wt.%) dissolved in *n*-hexane onto stainless steel substrate. After the evaporation of the solvent, the electrodes were pressed and then dried under vacuum at 200 °C for 2 h. The cell comprised a carbon electrode, a separator and lithium metal electrode. The electrolyte used in the cell was 1 M $LiPF_6$ dissolved in the mixed solvents of PC: DMC (1:1 by volume). The charge–discharge procedures of the cells consisted of both the constant current and constant voltage modes. The cut-off voltages were 10 mV and 1.5 V, and the constant current density applied was 0.4 mA $cm^{-2}$. In the charge ($Li^+$ insertion into carbon) course, as the voltage of the cell arriving 10 mV after constant current mode, the cell was kept at this voltage for 48 h. In the discharge ($Li^+$ extraction from carbon) course,

only the constant current mode was utilized. The rest time between charge and discharge courses was 10 min.

## 3. Results and discussion

Table 1 lists the elemental analysis data of NSF-N. The experimental values of different elemental contents for NSF-N are very near to the theoretical values based on its structural formula.

Fig. 2 shows the thermal gravimetric curves of NSF-N and β-NS. For β-NS, there are two DTG weight-loss peaks at 300 and 370 °C, respectively. In the same temperature region, there is only one DTG weight-loss peak at 330 °C for NSF-N. Moreover, there is another DTG weight-loss peak at 560 °C for NSF-N, whereas similar DTG peak can hardly be observed in the same temperature region for β-NS. The carbonization yield was measured as the ratio percent of the final weight at 1000 °C to the original weight. The carbonization yield of NSF-N is 47.5 wt.%. By contrast, the carbonization yield of β-NS is rather low, about 25.7 wt.%. Thus it can be concluded that NSF-N has a higher carbonization yield mainly because of the condensation of naphthalene rings.

Table 1
Elemental analysis of NSF

| Weight percents | C | H | N | S | O |
|---|---|---|---|---|---|
| Theoretical | 55.7 | 4.6 | 5.9 | 13.5 | 20.3 |
| Experimental | 55.4 | 4.5 | 5.7 | 13.8 | 20.6 |

Structure Formula

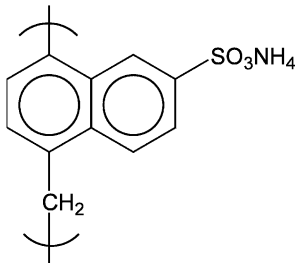


By the application of mass analysis apparatus, the decomposition gases generated in the above thermal analysis until 500 °C can be detected as illustrated in Fig. 3. The main components of the decomposition gases of β-NS are $NH_3$, $SO_2$, $H_2O$ and naphthalene. It can be expected that at the same time of the removal of $NH_3$ and $SO_2$, naphthalene became evaporated, which leaded to the low carbonization product of β-NS. Moreover, parts of $NH_3$ and $SO_2$ combined and formed ammonium sulfite, which decomposed once again at 370 °C and liberated $NH_3$, $SO_2$ and $H_2O$. On the other hand, the components of the decomposition gases for NSF-N are the same as those for β-NS. But little evaporation of naphthalene happened when $NH_3$ and $SO_2$ liberated at 330 °C, which might account for the higher carbonization yield for NSF-N. The carbonization yield of NSF-N was calculated to be 93.8 wt.% based on naphthalene starting material, which could prove that little naphthalene was evaporated during the heating scan.

From the above thermal and mass analysis, the carbonization process of NSF can be expected as shown in Fig. 4. At temperatures higher than 300 °C, $NH_3$ was liberated and the naphthalene sulfonic acid condensa-

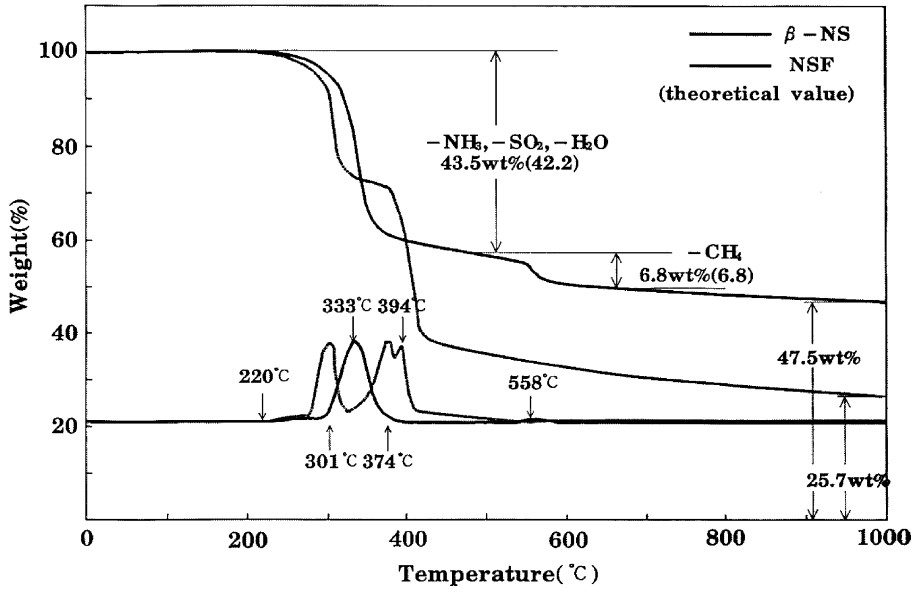


Fig. 2. Thermal gravimetric curves of NSF-N and β-NS.

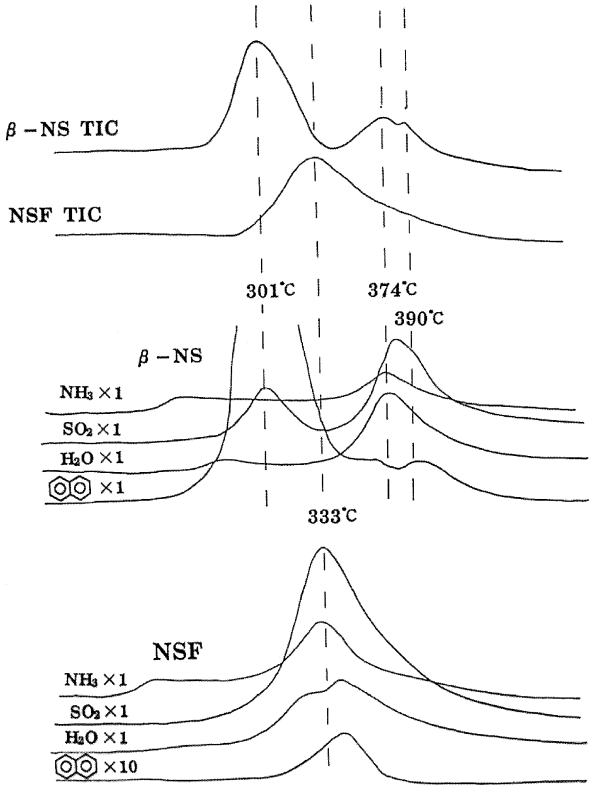


Fig. 3. Mass analysis of the decomposition gases generated in the thermal analysis of NSF-N and β-NS until 500 °C.

tion compound was formed. At higher temperatures, the sulfonic group decomposed and gave off $SO_2$. At this stage, NSF-N has similar structure with that of β-naphthol condensation compounds. At temperatures higher than 500 °C, with the water, methane and hydrogen liberation, the number of condensed benzene rings increased and the carbon skeleton thus formed. The above process is characteristic of the liberation of $NH_3$ and $SO_2$ at temperatures lower than 500 °C. Its carbonization process took place at temperatures higher than 500 °C, which is almost the same as that of phenol resin. The initial steps of alkali-melting of benzene sulfonic acid and hydrolysis in the synthesis route from phenol monomer to phenol resin can be replaced by the more convenient process from β-naphthalene sulfonic acid to β-naphthol in NSF-N synthesis.

Fig. 5 shows the DSC curve of NSF from room temperature to 600 °C. There is one big endothermic peak at 350 °C, the corresponding heat amounts to 800 J $g^{-1}$. We found that if being heated quickly to 400 °C in air, NSF would not be melted but solid-carbonized. This is because that in the course of quickly heating in air, much heat generated from the oxidation can be cancelled off by the endothermic reaction at 350 °C. This specific thermal feature could be used for the un-melting treatment in the formation of carbon micro-beads or fibers.

Fig. 6 shows the elemental analysis data of the NSF carbon beads. It can be seen that with the increase of carbonization temperature, the carbon content increases whereas other elements contents decreases. At temperatures higher than 500 °C, which point seems characteristic of NSF carbonization, there is little changes for the rations of the C, N and S contents. This fact implies that parts of the S and N atoms are included into the carbon skeleton. The binding of S to carbon is very stable even until the carbonization temperature as high as 1300 °C.

Almost all the carbonaceous materials fall into two categories: soft (graphitizable) and hard (non-graphitizable) carbons. Table 2 lists crystallographic parameters of NSF carbon beads heated at relatively high temperature. Even at heating temperature as high as 2800 °C, the crystal structure of NSF carbon beads cannot be considerably transformed into graphitic one yet, in terms of the relatively large $d_{002}$ and small $Lc_{(002)}$ values. In addition, at heating temperatures lower than 2000 °C, the diffraction peaks for (002) planes cannot be detected in the XRD patterns of NSF carbon beads at all. Thus NSF carbon beads can be assigned as a hard carbon.

Table 3 summarizes some physical properties of typical NSF carbon beads samples. From this table, it can be seen that NSF carbon beads have high bulk resistances, high compressive strengths, and high B.E.T. specific surface areas. Moreover, with the rise of carbonization temperature, the bulk resistance and B.E.T. specific surface area decline, whereas the density and the compressive strength grow up. Fig. 7 shows the SEM graph of NSF carbon beads carbonized at 1000 °C. The shapes of the carbon beads are regular sphere particles, and the surface morphology of the carbon beads appears very smooth.

Fig. 8 shows the typical charge curves of NSF carbon-beads. In the charge curves, the capacity of each carbon beads sample mainly falls into two voltage zones (from 1.4 to 0.3 V, and from 0.3 V to 10 mV). In the voltage range from approximately 1.4 to 0.3 V, each carbon beads sample roughly demonstrates a sloping curve. It seems that the slope of the charge curve in this potential range increases with the increase in carbonization temperature. In the voltage range from approximately 0.3 V to 10 mV, the slopes of the charge curves decrease as the lithium insertion proceeds and the charge curves level off at 10 mV due to the constant voltage modes we applied. For each NSF carbon beads samples, near half of the charge capacity falls on the constant voltage of 10 mV.

Fig. 9 shows the typical discharge curves of NSF carbon beads at the first cycle. The discharge curve of the carbon beads carbonized at 700 °C is quite different from those of other samples carbonized at higher temperatures. It has almost no plateau at voltages lower than 0.8 V. Instead, major part of the discharge capacity fall in the voltage range from 0.9 to 1.3 V, which has

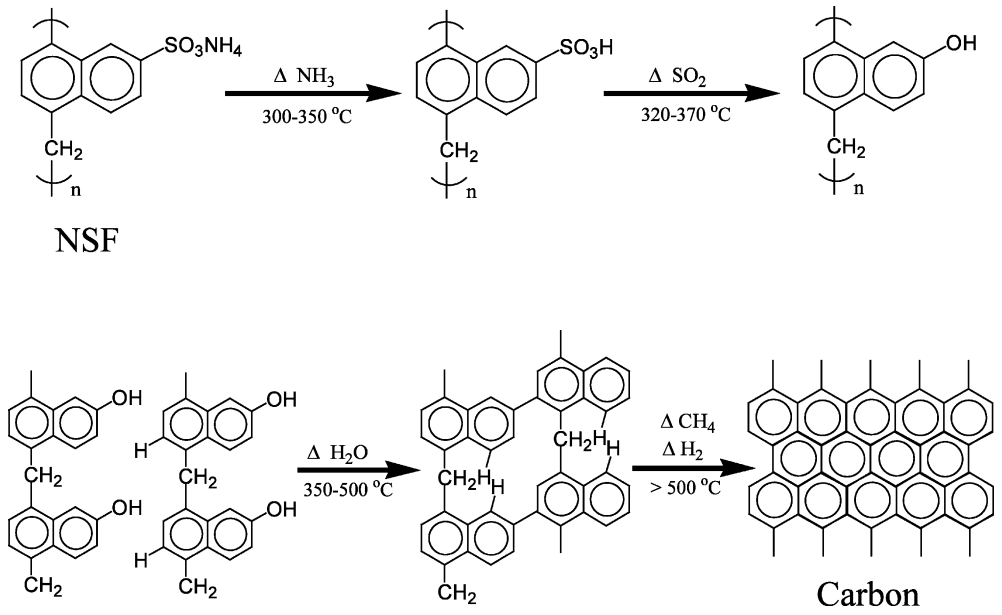


Fig. 4. Carbonization process of NSF.

been ascribed to lithium ions adsorbed at the edges of graphene layers [6] or lithium bond to H [7]. Although the discharge (reversible) capacity of NSF carbon beads carbonized at 700 °C is large (near 600 mA h $g^{-1}$), it proves insignificant use as an anode material in practical lithium-ion batteries because of its high average operation voltage against lithium metal, which may decrease the whole energy density. In the region between 700 and 1150 °C, as the carbonization temperature rises, the plateau at approximately 1.0 V becomes shortened and the plateau lower than 0.2 V appears lengthened. The contraction of the plateau at approximately 1.0 V with the rise in carbonization temperature may be ascribed to the H depletion with heating in nitrogen, whereas the appearance of plateau lower than 0.2 V can be explained in terms of lithium metal small clusters adsorbed in nanopores built by single graphene layers in hard carbon [8]. In the case of NSF carbon beads sample

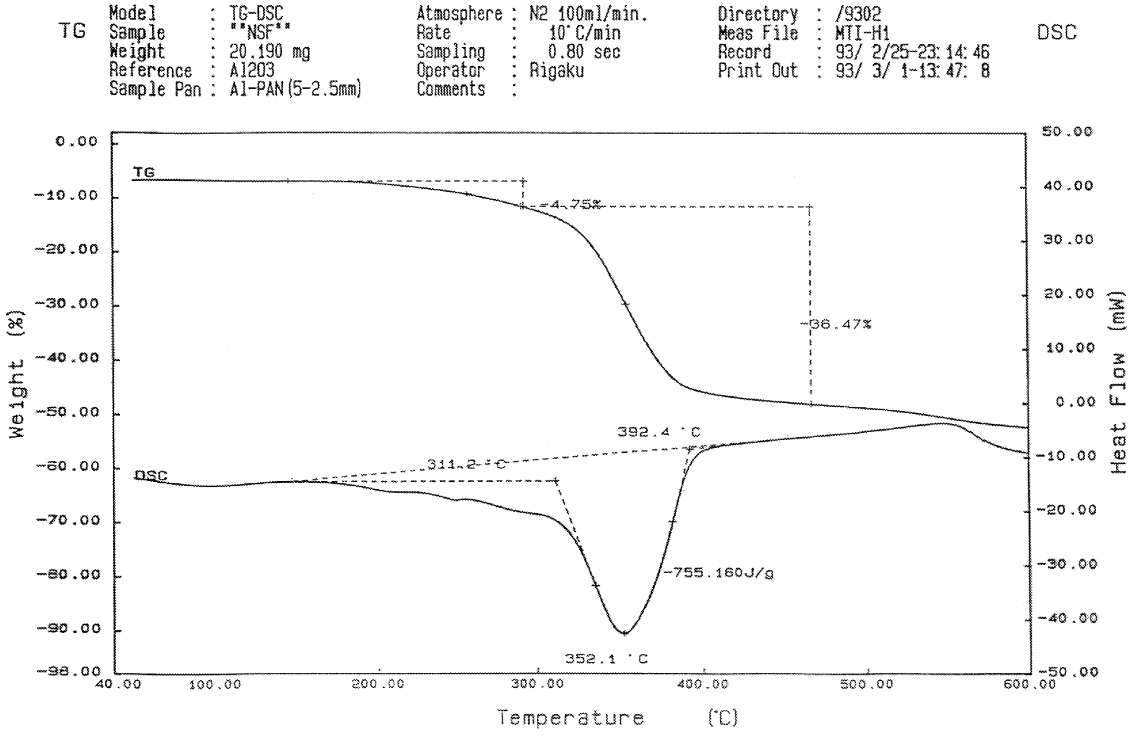


Fig. 5. DSC curve of NSF from room temperature to 600 °C.

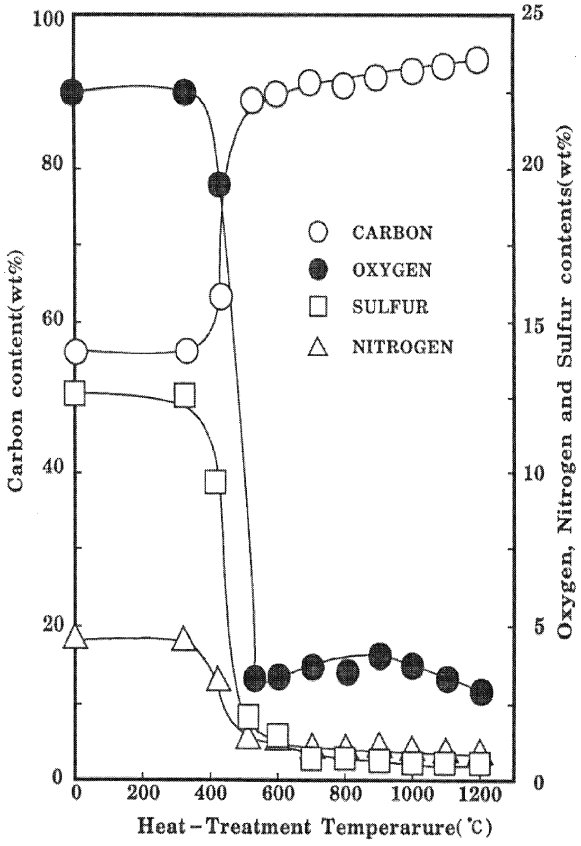


Fig. 6. Elemental analysis data of the NSF carbon beads.

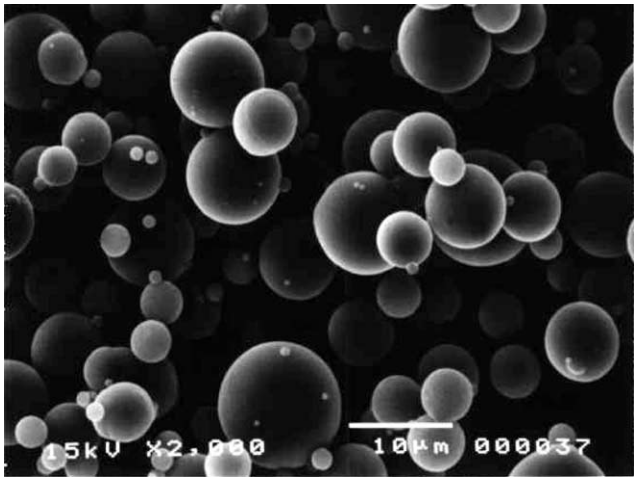


Fig. 7. SEM graph of NSF carbon beads carbonized at 1000 °C.

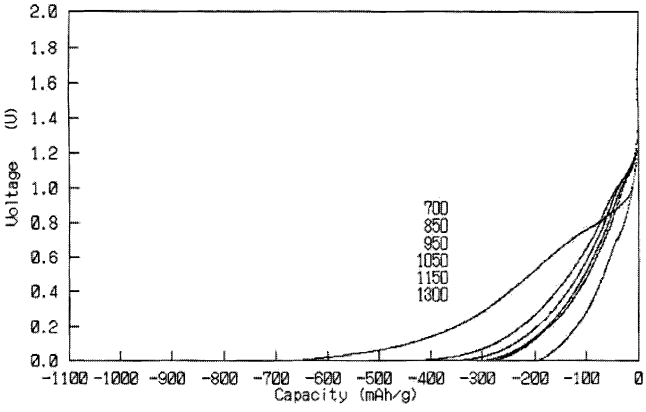


Fig. 8. Typical charge curves of NSF carbon-beads at the first cycle.

Table 2
Crystallographic parameters of NSF carbon beads carbonized at relatively high temperatures

| Carbonization temperature (°C) | $d_{002}$ (nm) | $Lc_{(002)}$ (nm) |
|---|---|---|
| 1300 | Not detectable | |
| 1600 | Not detectable | |
| 2000 | Not detectable | |
| 2400 | 0.3430 | 3.3 |
| 2600 | 0.3427 | 3.8 |
| 2800 | 0.3397 | 7.5 |

carbonized at 1300 °C, the capacity lower than 0.2 V is smaller than those of other samples (except 700 °C sample). This may be due to coalesce of single graphene layers or closure of the entrance into single-layer surrounded nano-pores after the high temperature heating.

Actually, for the preparation of suitable hard carbon anode materials for lithium-ion batteries, design of the NSF carbon beads can be carried out from the very beginning step: the adjustment of the molecular struc-

Table 3
Physical Properties of typical NSF carbon beads

| Carbonization temperature (°C) | Density (g $cm^{-3}$) | Bulk resistance (Ω cm) | Compressive strength (kgf $mm^{-2}$) | B.E.T. specific surface area ($m^2$ $g^{-1}$) |
|---|---|---|---|---|
| 600 | 1.40 | $3.11 \times 10^6$ | 70 | 48 |
| 650 | 1.47 | $1.85 \times 10^3$ | 75 | 59 |
| 700 | 1.58 | 12.4 | 110 | 105 |
| 800 | 1.59 | 0.207 | 130 | 135 |
| 900 | 1.60 | 0.0795 | 145 | 7 |
| 1000 | 1.61 | 0.0631 | 175 | 3 |

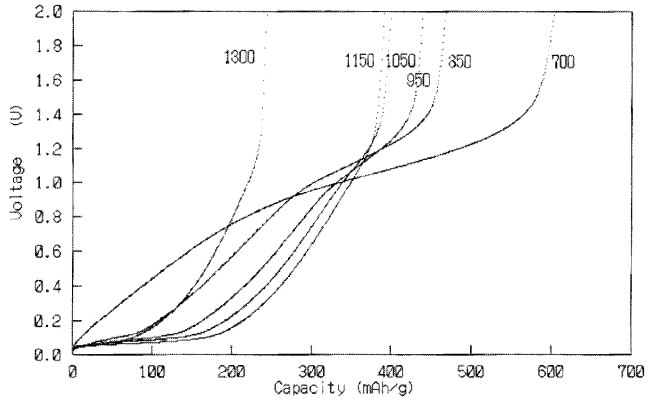


Fig. 9. Typical discharge curves of NSF carbon beads at the first cycle.

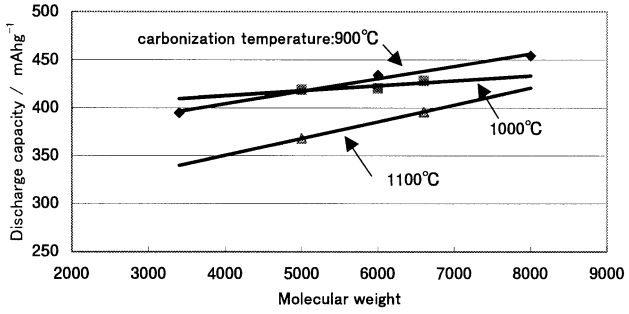


Fig. 10. Relationship between the reversible capacity and the molecular weight of precursor.

ture in the precursor. Fig. 10 shows the relationship between the reversible capacity and the molecular weight of precursor. It can be seen that for the carbonization temperatures of 900, 1000, 1100 °C, the reversible capacity of NSF carbon beads increases with the increase in molecular weight of the precursors. Moreover, the capacity increase with the increase in molecular weight mainly originates from the lengthening of the plateau lower than 0.2 V. Thus it seems that the high molecular weight precursor renders the enlargement of the single graphene layer dimensions and thus provide more residence sites for Li adsorption at low potential.

The ramp rate is also a key factor for controlling the performance of NSF carbon beads. Fig. 11 shows the relationship between the ramp rate and reversible capacity of NSF carbon beads. It can be seen clearly that the reversible capacity increases with increasing the ramp rate. It is assumed that higher ramp rates

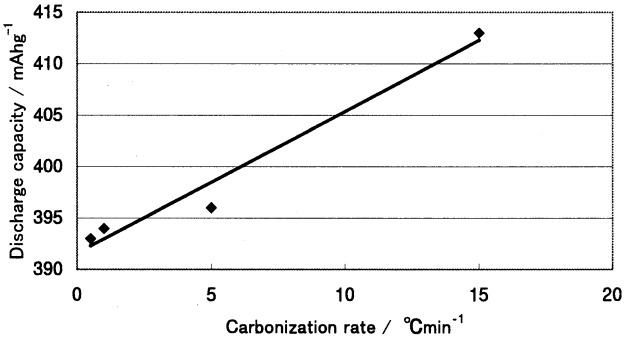


Fig. 11. Relationship between the ramp rate and reversible capacity of NSF carbon beads.

facilitates 'solidification' of the disordered structure in the precursor to the resultant carbon and obstacle the alignment of aromatic polymer segments into ordered graphitic structures which generally develops slowly under mild thermal treatment.

## 4. Conclusion

NSF-resin derived carbon beads, a typical hard carbon, has been prepared as an anode material for lithium-ion batteries. Carbonization conditions like final temperature, ramp rate, and molecular weight of the precursor play important roles in the performance of carbon beads.

## References

[1] T. Tanaka, K. Ohta, N. Arai, J. Power Sources 97–98 (2001) 2.
[2] M. Fujimoto, Y. Kida, T. Nohma, M. Takahashi, K. Nishio, T. Saito, J. Power Sources 63 (1996) 127.
[3] K. Tokumitsu, A. Mabuchi, H. Fujimoto, T. Kasuh, J. Electrochem. Soc. 143 (1996) 2235.
[4] H. Higuchi, K. Uenae, A. Kawakami, J. Power Sources 68 (1997) 212.
[5] Y. Mori, T. Iriyama, T. Hashimoto, S. Yamazaki, F. Kawakami, H. Shiroki, J. Power Sources 56 (1995) 205.
[6] H.Q. Xiang, S.B. Fang, Y.Y. Jiang, J. Electrochem. Soc. 144 (1997) L187.
[7] T. Zheng, W.R. McKinnon, J.R. Dahn, J. Electrochem. Soc. 143 (1996) 2137.
[8] W. Xing, J.S. Xue, T. Zheng, A. Gibaud, J.R. Dahn, J. Electrochem. Soc. 143 (1996) 3482.